Volume 1 | Number 1 | Jan 2013 | Pages 1–100

Chemical Science

www.rsc.org/chemicalscience

ROYAL SOCIETY OF CHEMISTRY

This is an *Accepted Manuscript*, which has been through the Royal Society of Chemistry peer review process and has been accepted for publication.

Accepted Manuscripts are published online shortly after acceptance, before technical editing, formatting and proof reading. Using this free service, authors can make their results available to the community, in citable form, before we publish the edited article. We will replace this *Accepted Manuscript* with the edited and formatted *Advance Article* as soon as it is available.

You can find more information about *Accepted Manuscripts* in the **Information for Authors**.

Please note that technical editing may introduce minor changes to the text and/or graphics, which may alter content. The journal's standard **Terms & Conditions** and the **Ethical guidelines** still apply. In no event shall the Royal Society of Chemistry be held responsible for any errors or omissions in this *Accepted Manuscript* or any consequences arising from the use of any information it contains.

Journal Name

ARTICLE

Controlling Selectivity in the Reductive Activation of CO_2 by Mixed Sandwich Uranium(III) Complexes[†]

Nikolaos Tsoureas,[a] Ludovic Castro,[b] Alexander F. R. Kilpatrick,[a] F. Geoffey N. Cloke,*[a] and Laurent Maron.*[b]

The synthesis and molecular structures of a range of uranium(III) mixed sandwich complexes of the type $[U(\eta^8\text{-}C_8H_6(1,4\text{-}SiMe_3)_2)(\eta^5\text{-}Cp^{Me4R})]$ (R= Me, Et, ${}^iPr$, ${}^tBu$,) and their reactivity towards CO_2 are reported. The nature of the R group on the cyclopentadienyl ring in the former has a significant effect on the outcome of CO_2 activation: when R=Me, the products are the bridging oxo complex $\{U[\eta^8\text{-}C_8H_6(1,4\text{-}SiMe_3)_2](\eta^5\text{-}Cp^{Me5})\}_2(\mu\text{-}O)$ and the bridging oxalate complex $\{U[\eta^8\text{-}C_8H_6(1,4\text{-}SiMe_3)_2](\eta^5\text{-}Cp^{Me5})\}_2(\mu\text{-}\eta^2:\eta^2\text{-}C_2O_4)$; for R= Et or ${}^iPr$, bridging carbonate $\{U[\eta^8\text{-}C_8H_6(1,4\text{-}SiMe_3)_2](\eta^5\text{-}Cp^{Me4R})\}_2(\mu\text{-}\eta^2:\eta^1\text{-}CO_3)$ and bridging oxalate complexes $\{U[\eta^8\text{-}C_8H_6(1,4\text{-}SiMe_3)_2](\eta^5\text{-}Cp^{Me4R})\}_2(\mu\text{-}\eta^2:\eta^2\text{-}C_2O_4)$ are formed in both cases; and when R= ${}^tBu$ the sole product is the bridging carbonate complex $\{U[\eta^8\text{-}C_8H_6(1,4\text{-}SiMe_3)_2](\eta^5\text{-}Cp^{Me4tBu})\}_2(\mu\text{-}\eta^2:\eta^1\text{-}CO_3)$. Electrochemical studies on both the uranium(III) complexes and the dimeric uranium(IV) CO_2 reduction products have been carried out and all exhibit quasi reversible redox processes; in particular, the similarities in the U(III)/U(IV) redox couples suggest that the selectivity in the outcome of CO_2 reductive activation by these complexes is steric in origin rather than electronic. The latter conclusion is supported by a detailed computational DFT study on the potential mechanistic pathways for reduction of CO_2 by this system.

Introduction

The use of well-defined molecular species to activate small molecules has spearheaded advances in chemical transformations in an energy and atom efficient manner, and has expanded the scope of utilizing such small, abundant molecules to produce commodity and high-added value chemicals.[1] The emergence of CO_2 as a climate-changing small molecule coupled with the depletion of fossil fuels as feedstocks for the petrochemical industry and energy production, has led to significant amount of research into the use of CO_2 as a potential C1 feedstock.[2] For example, Milstein *et al.* have recently described how CO_2 can be chemically captured and then reduced to MeOH by H_2 under relatively mild conditions.[3] Other examples involve electrochemical approaches to the chemical transformation of CO_2,[4] frustrated Lewis pair capture and functionalization,[5] and transition metal catalysed CO_2 incorporation into organic substrates.[6]

In recent years, the use of organometallic uranium complexes for small molecule activation has attracted significant interest and advances towards uranium based catalysis have elevated these academically interesting molecules to a vibrant area of research.[7] Examples include the capture and reduction of dinitrogen,[8] the reductive coupling/oligomerisation of carbon monoxide,[9, 10] and the reductive coupling of CO/H_2 to methoxide.[11] In the specific case of CO_2, reduction to afford uranium oxo complexes and CO has been achieved using U(III) complexes incorporating tripodal tris(aryloxide)[12] or siloxide ligands,[13] and disproportionation to CO and uranium carbonate derivatives has been described for mixed sandwich U(III),[14] neutral and anionic U(III) siloxide,[13] and tris(aryloxide) systems.[15] Whilst the reductive coupling of CO_2 to the oxalate dianion may be achieved by reaction of CO_2 with molten alkali metals or their amalgams,[16] well defined molecular systems that will undergo this reaction are very rare.[17,18] Indeed, the best known example of clean, reductive coupling of CO_2 to the oxalate dianion remains that first reported by Evans several years ago using the divalent lanthanide complex $Sm(\eta^5\text{-}Cp^*)_2(THF)_2$,[19, 20] and later extended to other lanthanide metal centres.[21] To the best of our knowledge such a transformation has not been previously reported using uranium or indeed any actinide metal centre. Herein we present the first example of the latter, and furthermore demonstrate the effect of the steric environment around the uranium centre in guiding the possible reductive

transformation pathways of CO_2 (*i.e.* reductive coupling, reductive disproportionation, or reduction).

Results and Discussion

Synthesis of U(III) complexes

Since we had previously demonstrated the reductive disproportionation of CO_2 by $[U(\eta^8\text{-}C_8H_6(1,4\text{-}Si^iPr_3)_2)(\eta^5\text{-}Cp^{Me4R})(THF)]$ (R=Me, H),[14] our initial attempts to promote alternative reductive pathways (i.e. reduction or coupling) for CO_2 activation focussed on variants of the former incorporating more sterically demanding cyclopentadienyl groups (e.g. R= Et, ^iPr, $SiMe_3$[10]). However, in all cases reaction with CO_2 resulted in extensive decomposition of the starting U(III) complexes and no tractable products arising from the reductive activation of CO_2 could be obtained. Having recently established that U(III) mixed sandwich complexes incorporating the bis(tri*methyl*silyl) substituted COT ligand and an appropriately substituted Cp ligand were effective for the reductive oligomerisation of CO, we decide to turn our attention to a study of the reactivity of compounds of this type (i.e. $[U(\eta^8\text{-}C_8H_6(1,4\text{-}SiMe_3)_2)(\eta^5\text{-}Cp^{Me4R})(THF)x])$ towards CO_2.[10] The synthesis of the latter U(III) complexes is outlined in Scheme 1 and the new compounds **2-4** can be isolated in moderate yields as black-brown crystalline solids, as previously described for **1a** and **1b**.[10, 22]
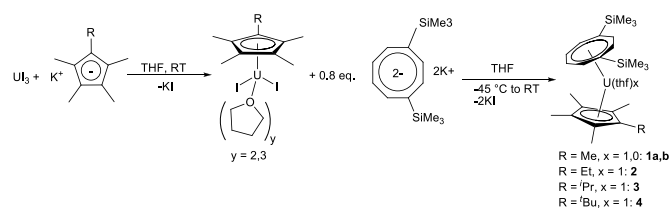
Scheme 1: Synthesis of complexes $\{U[\eta^8\text{-}C_8H_6(1,4\text{-}SiMe_3)_2](\eta^5\text{-}Cp^{Me4R})(THF)_x\}$ **1-4**.

The new mixed sandwich compounds **2-4** displayed the expected paramagnetically shifted ^1H and $^{29}Si\{^1H\}$ NMR spectra and their their mass spectra (EI mode) showed the parent ions $(M)^+$ with isotopic distributions in agreement with the calculated isotopic envelopes. Unfortunately, **2-4** are temperature sensitive even in the solid state and therefore reliable elemental analyses could not be obtained. However, their molecular formulations were unambiguously confirmed by single crystal X-ray diffraction studies.

Figure 1 shows the ORTEP diagrams of the molecular structures for **2**, **3** and **4**, and U−COTcentroid, U−Cpcentroid, U-O(THF) distances (Å) and COTcentroid−U−Cp centroid angles (°) are given in Table 1. The molecular structure of **1b** has been previously described and therefore is not included here.[10]
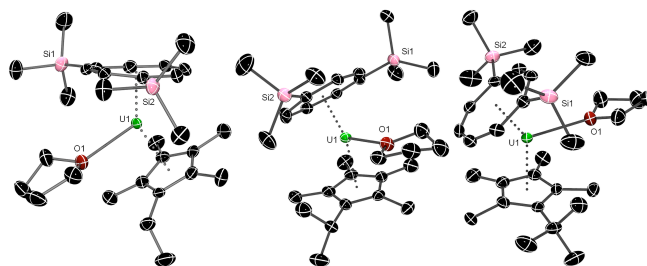

Figure 1: From left to right, ORTEP diagrams (50% probability ellipsoids) of the molecular structures of (**2**), (**3**) and (**4**) (hydrogen atoms and Me substituents of the $SiMe_3$ groups of **2** have been omitted for clarity).

	U-COT$_{cent.}$	U-Cp^{Me4R}$_{cent.}$	U-O	COT$_{cent.}$-U-Cp^{Me4R}$_{cent.}$
1b	1.971(15)	2.440(15)	n/a	139.1(6)
2	1.9708(4)	2.482(4)	2.602(4)	144.31(7)
3	1.977(9)	2.502(8)	2.589(7)	143.9(3)
4	1.982(9)	2.511(8)	2.615(8)	141.9(3)

Table 1: Important distances (Å) and angles (°) for complexes **1b-4**.

All the complexes **1-4** are isostructural, exhibiting a bent sandwich structure, and in the case of **1a** and **2-4** a THF coordinated molecule. Within e.s.ds, the U-COT centroid distances are the same within the series, as are the U-O(THF) bond lengths. The U-Cp^{Me4R} centroid distance in **3** (R = ^iPr) is longer than the corresponding one in **2** (R = Et) but similar within e.s.ds to that in **4** (R = ^tBu). Similarly, the U-Cp^{Me4R} centroid distance in **2** is longer than that found in **1b** (R = Me). Finally, it is worth noting that the COT centroid-U-Cp^{Me4R} centroid angle decreases with increasing steric bulk of the R substituent moving down the series from (**2**) (R = Et) to (**4**) (R = ^tBu).

Reactivity with CO_2.

Addition of 1-3 eq of $^{13}CO_2$ (administered accurately *via* a Toepler pump) to a d^8-toluene solution of (**1a**) at -78 °C followed by slow equilibration to room temperature resulted in the formation of a brick-red precipitate with a bright red supernatant solution. The ^1H-NMR spectrum of the supernatant showed one major species, but no ^{13}C-labelled signals could be located in its $^{13}C\{^1H\}$-NMR spectrum. A clue to the identity of this species was provided by the $^{29}Si\{^1H\}$-NMR spectrum which consisted of two peaks at -108.65 and -103.76 ppm suggesting a non centrosymmetric structure. Such a characteristic spectrum has been observed in the case of the μ-oxo complex $\{U[\eta^8\text{-}C_8H_6(1,4\text{-}Si^iPr_3)_2](\eta^5\text{-}Cp^{Me5})\}_2(\mu\text{-}O)$, prepared from the reaction of $\{U[\eta^8\text{-}C_8H_6(1,4\text{-}Si^iPr_3)_2](\eta^5\text{-}Cp^{Me5})THF\}$ with a mixture of NO/CO.[23] This suggested that reduction of CO_2 by (**1a**) had occurred to form $\{U[\eta^8\text{-}C_8H_6(1,4\text{-}SiMe_3)_2](\eta^5\text{-}Cp^{Me5})\}_2(\mu\text{-}O)$ (**6**). This was verified by a single crystal X-ray diffraction study on crystals of (**6**) obtained from

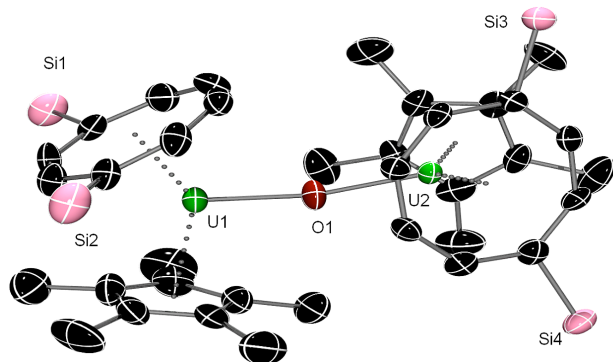n-pentane (-35 °C). Figure 2 shows the ORTEP diagram of the molecular structure of (**6**).

Figure 2: ORTEP diagram of the molecular structure of (**6**) with 50% probability ellipsoids. Hydrogen atoms and methyl groups of the $SiMe_3$ substituents have been removed for clarity. Selected bond lengths (Å) and angles (°): U1-COT$_{centroid}$ 1.955(4), U1-Cp$^{Me5}_{centoid}$ 2.519(5), U2-Cp$^{Me5}_{centroid}$ 2.538(4), U2-COT$_{centroid}$ 1.961(4), O1-U1 2.104(4), O1-U2 2.117(5); U1-O1-U2 159.6(3), COT$_{centroid}$-U1-Cp$^{Me5}_{centroid}$ 139.7(16), COT$_{centroid}$-U2-Cp$^{Me5}_{centroid}$ 140.0(16).

The asymmetric unit of the molecular structure of (**6**) contains two molecules with almost identical metric parameters apart from the U-O-U bond angle which is found to be 159.6(3)° and 161.2(2)°. The reason for this is unclear. The U-O bond distances are essentially the same with those previously reported for $\{U[\eta^8\text{-}C_8H_6(1,4\text{-}Si^iPr_3)_2](\eta^5\text{-}Cp^{Me5})\}_2(\mu\text{-}O)$, but the U-O-U angle, even though still deviating from linear as in the case of $[U(\eta^5\text{-}C_5H_5)_3]_2(\mu\text{-}O)$, is less acute than in $\{U[\eta^8\text{-}C_8H_6(1,4\text{-}Si^iPr_3)_2](\eta^5\text{-}Cp^{Me5})\}_2(\mu\text{-}O)$ (159.6(3)° and 161.2(2)° in (**6**) *vs* 154.5(3)°). The dihedral angle of the planes defined by the COT$_{centroid}$-U-Cp$^{Me5}_{centroid}$ vectors also deviates slightly from orthogonal in (**6**) (86.59(5)°), unlike $\{U[\eta^8\text{-}C_8H_6(1,4\text{-}Si^iPr_3)_2](\eta^5\text{-}Cp^{Me5})\}_2(\mu\text{-}O)$ where the corresponding angle is essentially orthogonal (89.07(2)°). This could be due to the influence of the smaller methyl silyl substituents in (**6**); all other metric parameters are essentially similar and therefore will not be discussed further.

The brick-red precipitate from the reaction mixture proved to be insoluble in most common (and compatible) organic solvents at ambient temperature. Never the less it was soluble enough in boiling mesitylene and upon filtration of a hot solution followed by cooling at room temperature provided crystals suitable for a single-crystal X-ray diffraction study. Most interstingly, these proved to be the oxalate dimer $\{U[\eta^8\text{-}C_8H_6(1,4\text{-}SiMe_3)_2](\eta^5\text{-}Cp^{Me5})\}_2(\mu\text{-}\eta^2\text{:}\eta^2\text{-}C_2O_4)$ (**7**), whose molecular structure is shown in Figure 3. To the best of our knowledge this is the first example of a reductive coupling of CO_2 on an actinide metal centre. The C-C distance of 1.54(3) Å is consistent with a single bond and is similar within esd's to those found in $[Ln(\eta5\text{-}CpMe4R)THF]_2(\mu\text{-}\eta^2\text{:}\eta^2C_2O_4)$ (Ln = Sm,

R = $SiMe_2CH_2CH=CH_2$;[20] Ln = Lu, R = H[21]), in $[\{Cu(tacn)allyl\}_2(\mu\text{-}\eta^2\text{:}\eta^2C_2O_4)]BPh_4$[18] and in the U(VI) anions $[\{UO_2(NO_3)_2\}_2(\mu\text{-}\eta^2\text{:}\eta^2C_2O_4)]^-$.[24] The C-O bond length and the O-C-O, O-C-C bond angles are the same within esd's to those in $Na_2C_2O_4$ and therefore will not be discussed further.[25] Due to the insolubility of (**7**) in common organic solvents, the acquisition of solution NMR data was not possible. However the mass spectrum showed the molecular ion at 1332 Da with an isotopic envelope agreeing with the proposed formula. v(CO) for (**7**) was located at 1583 cm^{-1} (Nujol mull) in (**7**)-^{13}C shifting to 1627.6 cm^{-1} in the (**7**)-^{12}C isotopomer as expected.[26]

When the reaction of (**1a**) with CO_2 is carried out at at *room temperature*, the oxalate (**7**) is not formed and the oxo bridged dimer (**6**) is isolated in high yields as the sole product. This means that the possible reductive pathways can be controlled thermodynamically or kinetically- the latter would suggest that careful manipulation of the steric environment around the reducing U(III) centre, might also affect the distribution of products of the three possible CO_2 reductive pathways.
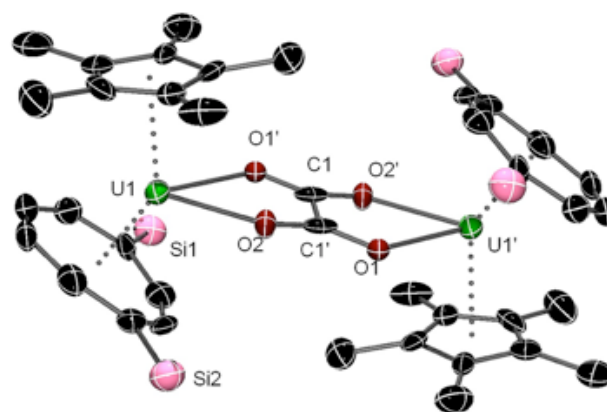

Figure 3: ORTEP diagram of the molecular structure of (**7**) with 50% probability ellipsoids. Hydrogen atoms and methyl groups of the $SiMe_3$ substituents have been omitted for clarity. Selected bond lengths (Å) and angles (°):U-COT$_{centroid}$ 1.942(5), U- Cp$^{Me5}_{centroid}$ 2.469(4), C1-O1' 1.257(15), C1-O2' 1.281(15), C1-C1' 1.54(3), O2-U1 2.421(8) , O1-C1 1.257(15), O1-U1 2.437(8); COT$_{centroid}$-U-Cp$^{Me5}_{centroid}$ 138.8(6), O1'-C1-O2' 127.7(12), O1'-C1-C1' 118.3(17), O2'-C1-C1' 114.0(16), C1-O1'-U1 118.9(9), O2-U1-O1' 66.3(3).

When (**2**) or (**3**) were reacted in a similar manner to (**1**) with [13]CO_2 at -78 °C, again formation of red precipitates was observed. Isolation of these solids by filtration followed by recrystallisation from hot (almost boiling) toluene led to the isolation of the bridging oxalate complexes $\{U[\eta^8\text{-}C_8H_6(1,4\text{-}SiMe_3)_2](\eta^5\text{-}Cp^{Me4Et})\}_2(\mu\text{-}\eta^2\text{:}\eta^2\text{-}C_2O_4)$ (**8**) and $\{U[\eta^8\text{-} C_8H_6(1,4\text{-}SiMe_3)_2](\eta^5\text{-}Cp^{Me4iPr})\}_2(\mu\text{-}\eta^2\text{:}\eta^2\text{-}C_2O_4)$ (**9**) respectively, which were characterised by spectroscopic and analytical methods. Unlike (**7**), both (**8**) and (**9**) are sufficiently soluble (warm d$_8$-toluene (50 °C) with a few drops of d$_8$-THF for (**8**) and d$_8$-THF for (**9**)) to obtain meaningful NMR data. Both display the expected ^{1}H-NMR spectra, with the oxalate ligands characterised by[13]C{^{1}H} NMR resonances at -43.74 ppm and -

32.81 ppm for (**8**)-^{13}C and (**9**)-^{13}C respectively. The molecular structures of both (**8**) and (**9**) were unequivocally confirmed by single crystal X-ray diffraction studies (Figure 4).[27]
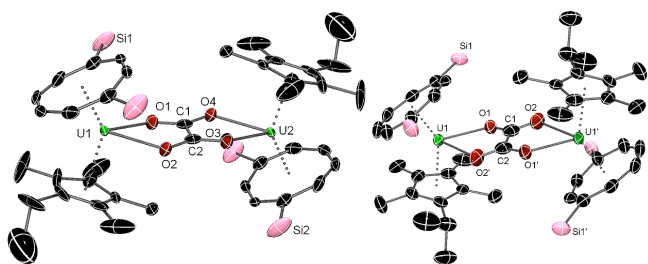

Figure 4: ORTEP diagram of the molecular structure of (**8**) (left) and (**9**) (right) with 50% probability ellipsoids. Hydrogen atoms and methyl groups of the SiMe$_3$ substituents have been omitted for clarity.

A comparison of key structural metrical parameters of (**7**), (**8**) and (**9**) is given in Table 2. In summary, all complexes have

The ^{13}C{^{1}H} NMR spectra of the crude reaction mixtures from the reactions of (**2**) and (**3**) with ^{13}CO$_2$ showed the presence of a second product in each case, in addition to the oxalate dimers (**8**) and (**9**), whose ^{13}C{^{1}H}NMR shifts were located at 44.09 and 69.49 ppm respectively. Mass spectral analysis of the crude products suggested these to be the
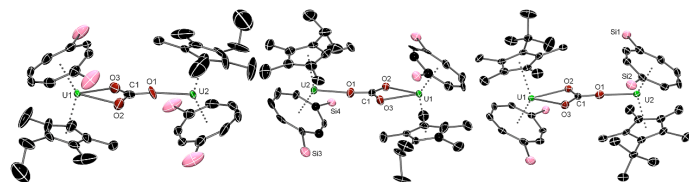

Figure 5: From left to right ORTEP diagrams of the molecular structures of (**11**), (**12**) and (**13**) with 50% probability ellipsoids. Hydrogen atoms and methyl groups of the SiMe$_3$ substituents have been omitted for clarity.

	{U[η^8-C$_8$H$_6$(1,4-SiMe$_3$)$_2$](η^5-Cp^{Me5})}$_2$(μ-η^2:η^2-C$_2$O$_4$) (**7**)	{U[η^8-C$_8$H$_6$(1,4-SiMe$_3$)$_2$](η^5-Cp^{Me4Et})}$_2$(μ-η^2:η^2-C$_2$O$_4$) (**8**)	{U[η^8-C$_8$H$_6$(1,4-SiMe$_3$)$_2$](η^5-Cp^{Me4iPr})}$_2$(μ-η^2:η^2-C$_2$O$_4$) (**9**)
U-COT$_{centroid}$	1.942(5)	1.951(3)	1.953(9)
U- Cp$^{Me4R}_{centroid}$	2.469(4)	2.454(4)	2.475(9)
COT$_{centroid}$-U-Cp$^{Me4R}_{centroid}$	138.8(6)	138.3(9)	143.1(3)
C1 O1	1.257(15)	1.261(6)	1.294(10)
C1 O2	1.281(15)	1.261(6)	1.222(10)
C1 C1'	1.540(3)	1.507(19)	1.476(16)
O1 U1	2.437(8)	2.431(4)	2.441(5)
O1 C1 O2	127.7(12)	126.7(9)	125.5(8)
O1 C1 C1'	118.3(17)	116.7(4)	115.2(10)
O2-U1-O1	66.3(3)	65.8(2)	65.6(2)

Table 2. Comparison of Bond Lengths (Å) and Angles (°) for (**7**), (**8**) and (**9**)

essentially the same metric parameters within esd's. The only salient differences can be found in (a) the more linear COT$_{centroid}$-U-Cp$^{Me4R}_{centroid}$ angle found in (**9**) compared to (**7**) and (**8**) attributed most likely to the increased steric hindrance of the ^{i}Pr group (in (**8**) the Et group can point away from the COT ligand thus releasing the steric strain) and (b) the reduction of the C-C bond length of the oxalate moiety in (**9**) compared to (**7**). Even though the reason for this is unclear, this bond length is still characteristic of a single C-C bond and is similar within esd's with previously reported structures containing the oxalate moiety.[20, 21, 24]

carbonate bridged dimers {U[η^8-C$_8$H$_6$(1,4-SiMe$_3$)$_2$](η^5-Cp^{Me4Et})}$_2$(μ-η^2:η^1-CO$_3$) (**11**), and {U[η^8-C$_8$H$_6$(1,4-SiMe$_3$)$_2$](η^5-Cp^{Me4iPr})}$_2$(μ-η^2:η^1-CO$_3$) (**12**). In both cases the proposed molecular formulae were verified by single crystal X-ray diffraction studies on crystals obtained by fractional crystallisation from a saturated THF solution in the case of (**12**) or from a saturated toluene solution in the case of (**11**) (Figure 5). The metrical parameters for (**11**) and (**12**) will be discussed together with those of (**13**), *vide infra*. It is worth noting that (**8**) and (**11**) both crystallise in the orthorhombic crystal system in

	$\{U[\eta^8\text{-}C_8H_6(1,4\text{-}SiMe_3)_2](\eta^5\text{-}Cp^{Me4Et})\}_2(\mu\text{-}\eta^1{:}\eta^2\text{-}CO_3)$ (11)	$\{U[\eta^8\text{-}C_8H_6(1,4\text{-}SiMe_3)_2](\eta^5\text{-}Cp^{Me4iPr})\}_2(\mu\text{-}\eta^1{:}\eta^2\text{-}CO_3)$ (12)	$\{U[\eta^8\text{-}C_8H_6(1,4\text{-}SiMe_3)_2](\eta^5\text{-}Cp^{Me4tBu})\}_2(\mu\text{-}\eta^1{:}\eta^2\text{-}CO_3)$ (13)
U1-COT$_{centroid}$	1.932(6)	1.944(5)	1.965(11)
U1-Cp$^{Me4R}_{centroid}$	2.435(10)	2.477(10)	2.503(12)
COT$_{centroid}$-U1-Cp$^{Me4R}_{centroid}$	138.4(10)	137.8(11)	136.7(4)
U2-COT$_{centroid}$	1.930(2)	1.929(5)	1.931(11)
U2-Cp$^{Me4R}_{centroid}$	2.470(11)	2.466(11)	2.461(11)
COT$_{centroid}$-U2-Cp$^{Me4R}_{centroid}$	139.1(13)	138.8(9)	139.5(4)
C1 O1	1.269(15)	1.307(19)	1.301(7)
C1 O2	1.282(8)	1.273(18)	1.288(7)
C1 O3	1.282(8)	1.270(17)	1.291(7)
O1 U2	2.207(8)	2.210(11)	2.216(5)
O2 U1	2.390(5)	2.406(10)	2.425(4)
O3 U1	2.390(5)	2.400(10)	2.391(4)
O2 C1 O1	121.4(6)	119.1(14)	120.1(6)
O3 C1 O1	121.4(6)	122.3(15)	122.2(6)
O2 C1 O3	117.2(11)	118.4(14)	117.6(5)
C1 O1 U2	174.2(8)	174.3(9)	175.4(5)

Table 3. Comparison of Bond Lengths (Å) and Angles (°) for **(11)**, **(12)** and **(13)**

the space groups *Cmca* and *Pnma* respectively with almost identical unit cell metrics. This might explain their propensity to co-crystallise, which in turn reduces the isolated yields of the pure compounds.

Unlike the reactivity of (**2**) and (**3**) towards CO_2 discussed so far, when CO_2 was admitted to a solution of $\{U[\eta^8\text{-}C_8H_6(1,4\text{-}SiMe_3)_2](\eta^5\text{-}Cp^{Me4tBu})THF\}$ (**4**), only one major product was detected in solution by ^{1}H-NMR and $^{13}C\{^1H\}$ NMR spectroscopy. The latter was of diagnostic value as it consisted of only one signal located at 84.46 ppm, in the same region of the spectrum as for (**11**) and (**12**), suggesting the formation of the analogous carbonate complex $\{U[\eta^8\text{-}C_8H_6(1,4\text{-}SiMe_3)_2](\eta^5\text{-}Cp^{Me4tBu})\}_2(\mu\text{-}\eta^2{:}\eta^1\text{-}CO_3)$ (**13**). The structure of the latter was confirmed by a single crystal X-ray crystallographic study (Figure 5). Table 3 provides comparison of the key metrics of complexes (**11**)-(**13**)

In all cases the carbonate moiety is essentially planar with the same key bond lengths and angles. The U-COT$_{centroid}$, U-CpMe4R$_{centroid}$ distances and COT$_{centroid}$-U-CpMe4R$_{centroid}$ angles are similar within esd's and even similar to the ones found in complexes (**7**), (**8**) and (**9**). In the case of (**12**) the asymmetric unit contains two molecules with similar metric parameters within esd's. Due to the disorder in the carbonate moiety in the previously reported $\{U[\eta^8\text{-}C_8H_6(1,4\text{-}Si^iPr_3)_2](\eta^5\text{-}Cp^{Me4H})\}_2(\mu\text{-}\eta^1{:}\eta^2\text{-}CO_3)\}$ a meaningful comparison is impossible, nevertheless the U-O bond distances are the same within esd's.[14]

The outcomes of the reactions of complexes (**1a**)- (**4**) with $^{13}CO_2$ are summarised in Figure 6. It should be noted that ^{13}CO should also be formed in all four reactions. In the case of **4** that forms exclusively the carbonate dimer, ^{13}CO is indeed observed

by NMR. However, in the case of **1-3** the reactions have to be filtered to remove the poorly soluble oxalate dimer prior to acquisition of NMR data, resulting in the escape of the ^{13}CO presumably formed.

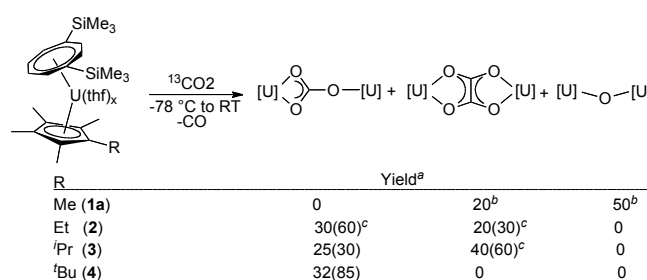| R		Yield^a	
Me (**1a**)	0	20^b	50^b
Et (**2**)	30(60)^c	20(30)^c	0
^{i}Pr (**3**)	25(30)	40(60)^c	0
^{t}Bu (**4**)	32(85)	0	0

Figure 6: Product distribution and isolated yields thereof from the possible reductive transformations of CO_2 promoted by complexes (**1a**)-(**4**). ^{a} Spectroscopic (NMR) yields in parenthesis; ^{b} spectroscopic yield not available due to insolubility of the oxalate dimer; ^{c} by relative integration of the $^{13}C\{^1H\}$ signals in solution-due to the poor solubility of the oxalate dimer, yields are biased in favour of the carbonate dimers.

Reactions in Supercritical CO_2

The reactions above were performed using typically 1-3 equivalents of CO_2 and the product distribution seemed to be unaffected by the gas stoichiometry. In order to probe the role of the gas concentration, the reactivity of complexes (**1a**)-(**4**) towards a massive excess of CO_2 using supercritical CO_2 (scCO_2) was studied. Although the complexes were not soluble in scCO_2, even in the solid state reaction occurred almost instantly as evidenced by a colour change from brown-black to deep red. Unfortunately, in the case of (**1a**) an intractable mixture was produced, but (**2**), (**3**) and (**4**) produced their respective (μ-η^2:η^1-CO_3) dimers (**11**), (**12**) and (**13**) very cleanly. More specifically in the case of (**3**) and (**4**) ^{1}H-NMR spectroscopy of the crude reaction mixtures showed only traces of decomposition and high conversion to the corresponding carbonate dimer. Evans has previously noted the merits of carrying out reactions of organo-f-element compounds with gases in the solid state in terms of product purity and yield.[28] Noticeably, in the case of (**3**) *ca.* only 5% of oxalate was identified in the reaction mixture, as opposed to the 40% obtained in the solution phase reaction- possibly due to a change in reaction kinetics as result of heterogeneous *versus* homeogenous reaction conditions.

Cyclic Voltametry (CV)

In order to investigate whether the observed selectivity of the above reactions is indeed only due to the differing steric environments imparted by the $CpMe_4R$ ligands and not to electronic effects (*ie* increasing +I effect with more electron rich ligands) electrochemical studies were performed on complexes (**1a**)-(**4**). Table 4 contains a summary of this study.

Compound {U[η^8-C$_8$H$_6$(1,4-SiMe$_3$)$_2$](η^5-Cp^{Me4R})(THF)$_x$}	[U^{III}] $\leftrightarrow$ [U^{IV}]$^+$ E$_½$ / V
R = Me (**1a**)	-2.10
R = Et (**2**)	-2.11
R = ^{i}Pr (**3**)	-2.02
R = ^{t}Bu (**4**)	-2.03

Table 4: Electrode potentials vs FeCp$_2$$^{+/0}$ in 0.05 M [^{n}Bu$_4$N][B(C$_6$F$_5$)$_4$] / THF.

All show a quasi-reversible process at *ca.* -2 V vs FeCp$_2$$^{+/0}$, which is within the expected range for the U^{III}/U^{IV} couple (detailed cyclic voltammograms are presented in the ESI). These potentials are all very similar, even though complexes (**1a**) and (**2**) seem to be slightly more reducing at first sight. Oxidation of U^{III} to [U^{IV}]$^+$ complexes results in an increase in transannular strain due to the smaller size of the U^{IV} ion. This is more significant for complexes with a more bulky Cp^{Me4R} ligand ie. R = ^{i}Pr (**3**) and ^{t}Bu (**4**), where sterics are at a premium, and hence a more positive E$_½$ (less reducing potential for U^{III}) is observed for these complexes. An analogous

argument has been used to rationalise the oxidation potentials of sterically hindered ferrocenes.[29][30] Hence, the similarities of the U^{III}/U^{IV} couples for all four complexes would suggest the non-involvement of electronic factors in determining the outcome of the CO_2 reductive pathways discussed above.

CV studies of the CO_2 reduction products [U^{IV}-(C$_x$O$_y$)-U^{IV}] were also undertaken, and are summarised in Table 5. All show two quasi-reversible processes within the electrochemical window. Process 1 is assigned to the [U^{IV}-U^{IV}]/[U^{IV}-U^{III}]$^-$ reduction, and occurs at a more negative potential than the U^{III}/U^{IV} oxidation process in the parent complex, indicating the U^{IV} centres are relatively stabilised by the bridging [C$_x$O$_y$]$^{2-}$ moiety.

Compound	Process 1 [U^{IV}-U^{IV}] $\leftrightarrow$ [U^{IV}-U^{III}]$^-$ E$_½$$^{(1)}$ / V	Process 2 [U^{IV}-U^{III}]$^-$ $\leftrightarrow$ [U^{III}-U^{III}]$^{2-}$ E$_½$$^{(2)}$ /V	ΔE$_½$$^{(1)-(2)}$/V
[**2**]$_2$(CO$_3$) (**11**)	-2.17	-2.85	0.68
[**3**]$_2$(C$_2$O$_4$) (**9**)	-2.15	-2.63	0.48
[**3**]$_2$(CO$_3$) (**12**)	-2.11	-2.78	0.67
[**4**]$_2$(CO$_3$) (**13**)	-2.12	-2.79	0.67

Table 5: Electrode potentials of some of the [U^{IV}-(C$_x$O$_y$)-U^{IV}] synthesised vs FeCp$_2$$^{+/0}$ in 0.1 M [^{n}Bu$_4$N][PF$_6$] / THF (actual voltammograms are presented in the ESI).

Process 2 is assigned to the [U^{IV}-U^{III}]/[U^{III}-U^{III}] reduction, and requires a significantly greater negative potential for carbonate complexes (**11**), (**12**) and (**13**), compared with oxalate complex (**9**). ΔE$_½$$^{(1)-(2)}$ for (**11**), (**12**) and (**13**) are noticeably larger than that for complex (**9**), consistent with a greater interaction between the two U centres in the mixed valence state for the carbonate bridged complexes compared with the oxalate case. The cyclic voltammogram of (**9**) as a typical example is shown in Figure 7.
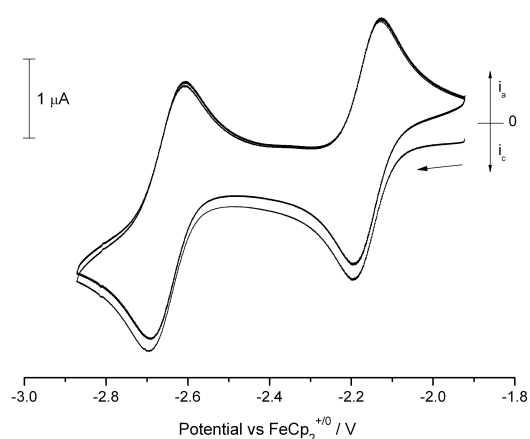

Figure 7: Overlaid CV scans (3 cycles) of {U[η^8-C$_8$H$_6$(1,4-SiMe$_3$)$_2$](η^5-Cp^{Me4iPr})}$_2$(μ-η^2:η^2-C$_2$O$_4$)} (**9**) in 0.1 M [^{n}Bu$_4$N][PF$_6$] / THF. Scan rate 100 mV s^{-1}.

To the best of our knowledge this is one of the few examples of such a study.[31, 32, 33, 34, 35, 36] The two quasi-reversible reduction processes observed for (**9**) suggests that the anionic complexes [**9**]$^-$ and [**9**]$^{2-}$ are stable on the timescale of the CV experiment,[37] and may be chemically accessible by reaction with a strong reducing agent.[38]

Computational Studies

In order to gain further insight into the mechanisms of the reactions observed experimentally, DFT calculations have been undertaken. Previous theoretical studies from our group have identified two possible reaction mechanisms for the formation of a dimeric bridging carbonate complex (Scheme 3).[39,40,41,42] The first step in both of them is the formation of a bimetallic complex with a doubly reduced to CO_2^{2-} moiety bridging two oxidized U(IV) centers (the one-electron reduced monomeric species LU-OCO was considered , but is some 35 kcal mol^{-1} higher in energy than the dimer). This key intermediate has been determined as the starting point for both possible pathways leading to bimetallic carbonate complexes. In mechanism **M1** (Scheme 3), loss of carbon monoxide forms a μ-oxo bimetallic species that reacts with another CO_2 molecule to form the observed carbonate dimer. Lam *et al.* have shown experimentally that this mechanism operates in the reaction of [((^{tBu}ArO)$_3$mes)U^{III}] with CO_2.[39] The other pathway, labeled mechanism **M2** in Scheme 3, proceeds via the electrophilic addition of a second CO_2 molecule on LU^{IV}-CO_2-LU^{IV} to form an unstable cyclic intermediate which readily looses CO to form the carbonate product. Most interestingly when the LU fragment was replaced by Cp*$_2$Sm^{II}, the analagous key intermediate Cp*$_2$Sm^{III}-CO_2-Cp*$_2$Sm^{III} was also observed and was found to react with a second molecule of CO_2 to yield the corresponding bimetallic oxalate complex *via* C-C coupling (mechanism **M3**). [19, 39]

Scheme 3: Summary of the three pathways of reduction of CO_2 by a U(III) complex. L stands for the set of ligands.
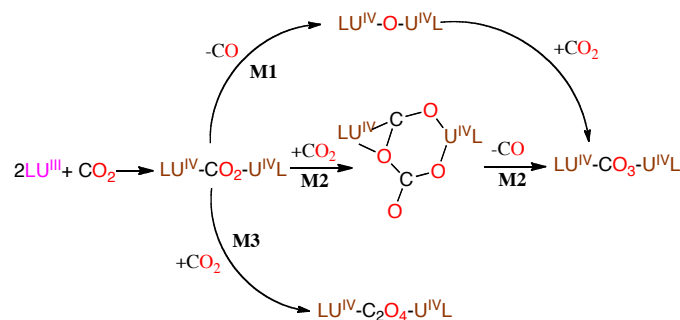
These three mechanisms were investigated theoretically for two of the uranium (III) complexes, namely [U(η^8-C$_8$H$_6${SiMe$_3$-1,4}$_2$)(η^5-C$_5$Me$_5$)] (**1**) and [U(η^8-C$_8$H$_6${SiMe$_3$-1,4}$_2$)(η^5-C$_5$Me$_4$(^{t}Bu))] [(**4**)-THF]. The coordinated THF has been excluded, as the first step of all pathways is the coordination of CO_2 to the uranium center following the displacement of the THF molecules. The mechanisms were also computed with the simpler model complex [U(η^8-C$_8$H$_6${SiH$_3$-1,4}$_2$)(η^5-C$_5$H$_5$)] to provide reference energy profiles when no significant steric repulsion is present. [U(η^8-C$_8$H$_6${SiMe$_3$-1,4}$_2$)(η^5-C$_5$Me$_5$)], [U(η^8-C$_8$H$_6${SiMe$_3$-1,4}$_2$)(η^5-Cp^{Me4tBu})] and [U(η^8-C$_8$H$_6${SiH$_3$-1,4}$_2$)(η^5-C$_5$H$_5$)] will be labeled **1_Me**, **1_tBu** and **1_H** respectively in this theoretical study. As mentioned above the first step involves the 2e$^-$ reduction of a CO_2 molecule where the CO_2^{2-} moiety is bridging two U(IV) metal centres. The methodology used to compute this oxidation step has been described previously for uranium and samarium complexes.[43, 44] For both systems **1_Me** and **1_tBu**, two structural conformations of this key intermediate were optimized, depending on the orientation of the ligands (Figure 8 for R=Me).
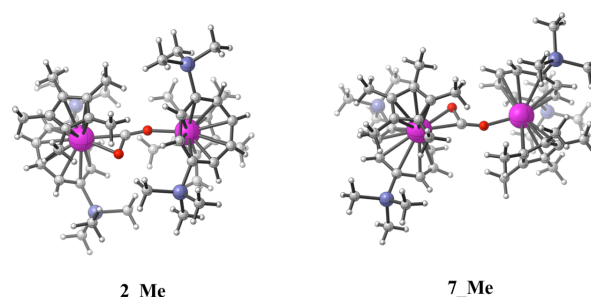

2_Me   **7_Me**

Figure 8: Structures of the key intermediates **2_Me** and **7_Me**; structures **2_tBu, 2_H** and **7_tBu** are qualitatively similar. (uranium : pink, carbon : grey, hydrogen = white, oxygen = red, silicon = blue)

In the first confirmation (complex **2_R**), the silyl groups of the COT ligands point towards the equatorial plane (where the CO_2^{2-} moiety is lying) and the COT ligand of one uranium center faces the Cp* ligand of the other uranium center in the dimer. The molecular structures of the carbonate and oxalate dimers display such a conformation and therefore **2_R** will be the starting point to study the mechanisms of their formation. In the second conformation (**7_R**), the silyl groups point outwards away from the bridging $CO.^{2-}$ moiety, while the two $[[U(\eta^8\text{-}C_8H_6\{SiR_3\text{-}1,4\}_2)(\eta^5\text{-}Cp^R)]$ fragments of the dimer are rotated by around 90° with respect to each other. The experimentally obtained μ-oxo products exhibit this conformation, and so **7_R** will be the starting point to study its mechanism of formation. In all structures, the CO_2 moiety is bent by around 116° and the C-O bond lengths have increased from 1.17 Å in free CO_2 to around 1.30 Å, which is consistent with a doubly-reduced carbon dioxide CO_2^{2-} in a singlet electronic ground state (for which the computed C-O bond lengths are 1.34 Å and the O-C-O angle is 115°). The coordination mode is $\mu\text{-}\eta^1{:}\eta^2$ because of the steric bulk of the ligands. The formations of **2_R** and **7_R** from two **1_R** complexes and one CO_2 molecule are exergonic by -16.1 and -13.4 Kcal/mol respectively for R=Me, and by -20.5 and -17.1 Kcal/mol respectively for R=tBu. Thus, we will assume that both configurations **2_R** and **7_R** can be formed at the beginning of the reactions. The simplified system **2_H** adopts a $\mu\text{-}\eta^2{:}\eta^2$ coordination mode, which has been observed in the reaction of $[(^{Me}ArO)_3mes)U^{III}]$ with CO_2.[39][39] This is due to the absence of steric congestion between the ligands which

allows a shorter U-U distance (5.01 Å) than in **2_Me** (6.11 Å). Therefore, as a result of the favorable U-O interactions and the absence of steric repulsion, the energy of formation of **2_H** is exergonic by -34.1 Kcal/mol. Thereafter, all free energy profiles will be shifted in order to put **2_R** and **7_R** as the zero of energy.

As a reference, the free energy profile of mechanism **M1** was computed with the simplified version of the complex, $[U(\eta^8\text{-}C_8H_6\{SiH_3\text{-}1,4\}_2)(\eta^5\text{-}C_5H_5]$, **1_H**. Free energy profiles for mechanisms **M2** and **M3** were also computed with **1_H**, but will not be discussed in detail. The free energy profile of mechanism **M1** is presented in red (R=H) in Figure 9, together with the structures corresponding to the stationary points for R=Me.

The first step of the reaction is the breaking of a weakened C-O bond of **2_H** (transition state **TS1_H**). The barrier height is calculated to be +8.4 Kcal/mol and the formation of the bridging linear μ-oxo complex **4_H** with concomitant release of CO is exergonic by -3.6 Kcal/mol, both with respect to **2_H**. The last step of the reaction is the insertion of CO_2 in **4_H** (transition state **TS2_H**) to form the carbonate-bridged product **6_H**. The barrier height is calculated to be +3.6 Kcal/mol and the formation of **6_H** is exergonic by -26.0 Kcal/mol, both with respect to **4_H**. In **6_H**, the CO_3^{2-} moiety adopts a $\mu\text{-}\eta^2{:}\eta^2$ coordination mode, due to the lack of steric congestion between the ligands. An isomer of the carbonate complex has been computed with a $\mu\text{-}\eta^1{:}\eta^2$ coordination mode with this simplified set, but was found to be less stable than **6_H** by 13.8 Kcal/mol.
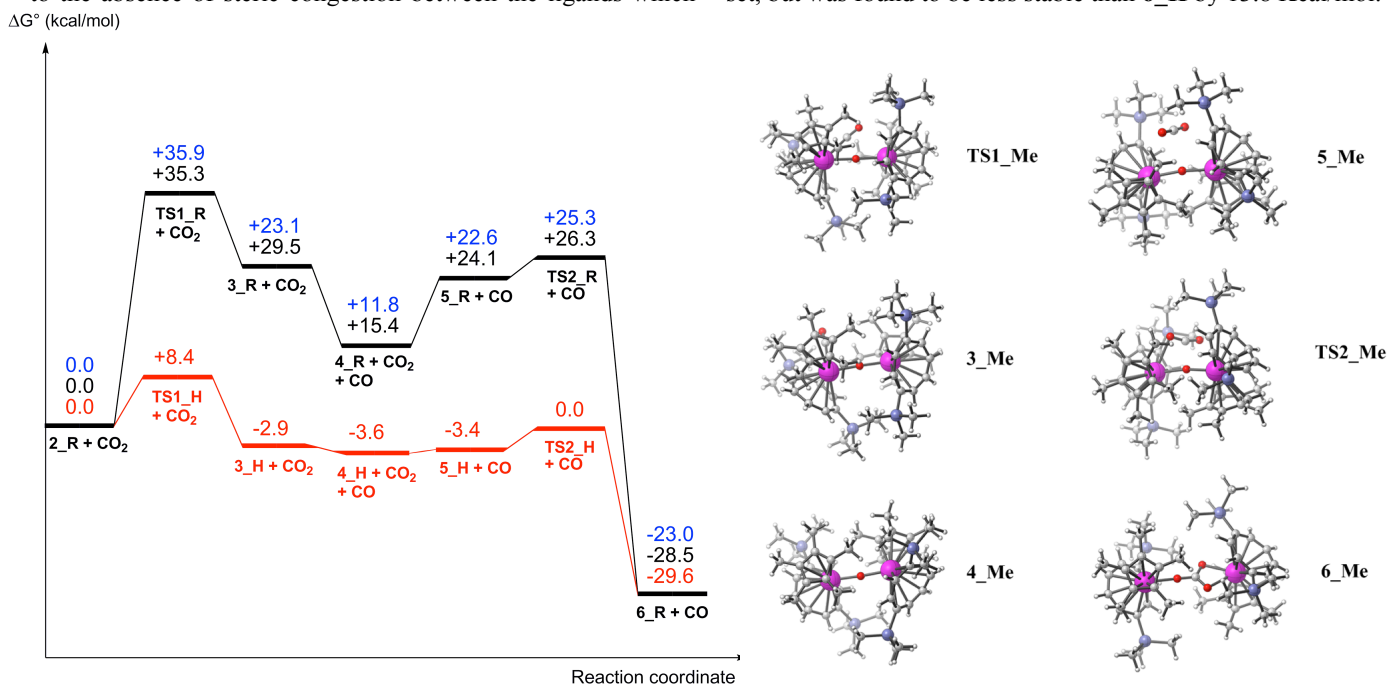

Figure 9. Computed free energy profile of mechanism **M1** between **1_R** (R = H in red, R = Me in blue, R = ^{t}Bu in black) and CO_2 (left), and computed structures for R=Me. Structures with R=tBu and R=H are qualitatively similar. (uranium : pink, carbon : grey, hydrogen = white, oxygen = red, silicon = blue)
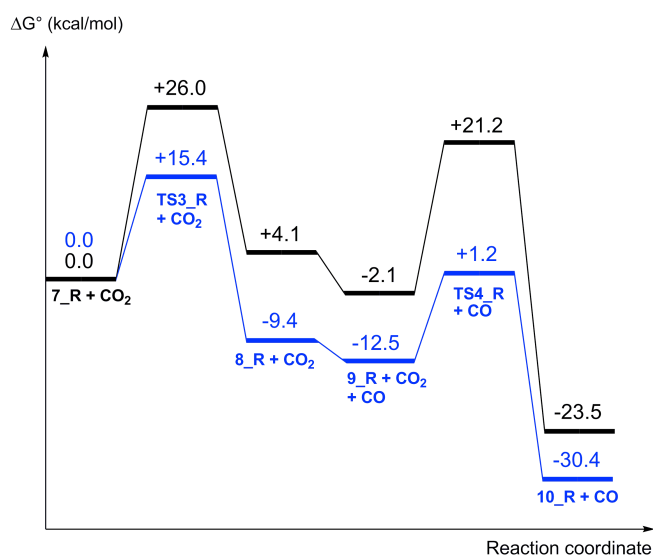
ΔG° (kcal/mol)

Figure 10: Computed free energy profile of reaction mechanism **M1** between **7_R** (R = Me in blue, R = ^{t}Bu in black) and CO_2.

In the case of **1_Me** the barrier height corresponding to the release of CO (**TS1_Me**) is calculated to be +35.9 Kcal/mol, with respect to **2_Me**. This high activation barrier kinetically prevents the formation of the μ-oxo intermediate **4_Me**. The modification of the ligands induces a strong destabilization; indeed, at the transition state level, the μ-oxo bridge is formed and thus the U-U distance decreases (from 6.07 Å in **2_Me** to 4.66 Å in **TS1_Me**), inducing high steric repulsion. Moreover, thermodynamically, the formation of **4_Me** is not favorable either (endergonic by +11.8 Kcal/mol), despite the loss of the very stable CO molecule and the concomitant gain of entropy. NBO and NPA analyses show that there are no important electronic differences between **TS1_H** and **TS1_Me** or between **4_H** and **4_Me** (see ESI Figure S5 for NPA charges) and demonstrates that these energetic differences are mainly due to steric effects.

The decrease of the U-U distance from 6.07 Å in **2_Me** to 4.40 Å in **4_Me** prevents the formation of the carbonate complex through mechanism **M1** despite the electrophilic attack of CO_2 on **4_Me** being kinetically accessible (**TS2_Me**, +13.5 Kcal/mol with respect to **4_Me**) and thermodynamically favorable (**6_Me**, -34.8 Kcal/mol with respect to **4_Me**). As expected due to the increased steric bulk when R = ^{t}Bu, both the release of CO and the formation of the μ-oxo dimer are endergonic and as a result the formation of the carbonate dimer through this mechanism is unfavourable.

When the starting key intermediate adopts conformation **7_Me** (Figure 8), the energy profile depicted in Figure 10 was calculated for mechanism **M1** (corresponding structures are presented in Figure S6 of the ESI).

The first activation barrier corresponding to the release of CO is lower that the one computed from the key intermediate **2_Me** (+15.4 Kcal/mol *versus* +35.9 Kcal/mol), probably because in **TS3_Me**, the U-O-U angle is bent (160°) (see ESI), while it is

linear in **TS1_Me**. Therefore, a *p*-type orbital pointing toward CO is developed on the bridging oxo stabilizing the transition state. Moreover, this conformation is more flexible and reduces the steric repulsion between the ligands. Thus, the breaking of the C-O bond becomes a kinetically accessible process. It is also a thermodynamically favorable reaction since the formation of **9_Me** is exergonic (-12.5 Kcal/mol) whereas it was endergonic for **4_Me** (+11.8 Kcal/mol). This first step shows that this μ-oxo complex **9_Me** can be formed *via* the reaction of **1_Me** with CO_2. The electrophilic addition of free CO_2 on the oxo group also seems favorable since the activation barrier is computed to be only +13.7 Kcal/mol and the formation of the carbonate product **10_Me** with concomitant release of CO is exergonic by -17.9 Kcal/mol, both with respect to **9_Me.**

In the case where R = ^{t}Bu, the activation barrier corresponding to the release of CO is calculated to be higher than for **7_Me** (+26.0 Kcal/mol vs +15.4 Kcal/mol). At the transition state level, the steric hindrance is higher with R = ^{t}Bu and to reduce it, the U-U distance has to become longer (from 4.79 Å in **TS3_Me** to 4.86 Å in **TS3_tBu**). This can only be achieved by opening the U-O-U angle (from 163.5° in **TS3_Me** to 168.7° in **TS3_tBu**). As already seen above and in previous studies,[39] the more the U-O-U angle is bent, the lower the activation barrier becomes due to the better orientation of a p-orbital on the oxygen atom stabilizing the O^{2-}-CO interaction. This in combination with the increased steric bulk in **TS3_tBu**, compared to **TS3_Me**, increases the activation barrier. As a consequence, the formation of the μ-oxo complex is also less thermodynamically favorable (-2.1 Kcal/mol).

As shown in Scheme 3, the carbonate dimers can also be accessed *via* pathway **M2**. The calculated free energy profile of this mechanism is presented in Figure 11, together with the corresponding geometries.

After the formation of the key intermediate **2_Me**, electrophilic addition of free CO_2 at one of the nucleophilic oxygen of the CO_2^{2-} moiety gives rise to **12_Me** *via* **TS5_Me**. Since the U-U distance remains long at the transition state (6.49 Å), there is no steric repulsion and the activation barrier, with respect to **2_Me**, is equal to +10.6 Kcal/mol. It is noteworthy that the activation barrier is exactly the same for **TS5_H**, proving that **TS5_Me** is not destabilized by any steric hindrance. Intermediate **12_Me** features an unstable six-member ring where a C-O bond has been formed between the carbon of CO_2 and the oxygen of CO_2^{2-} and readily looses a molecule of CO *via* **TS6_Me**, to form the bimetallic
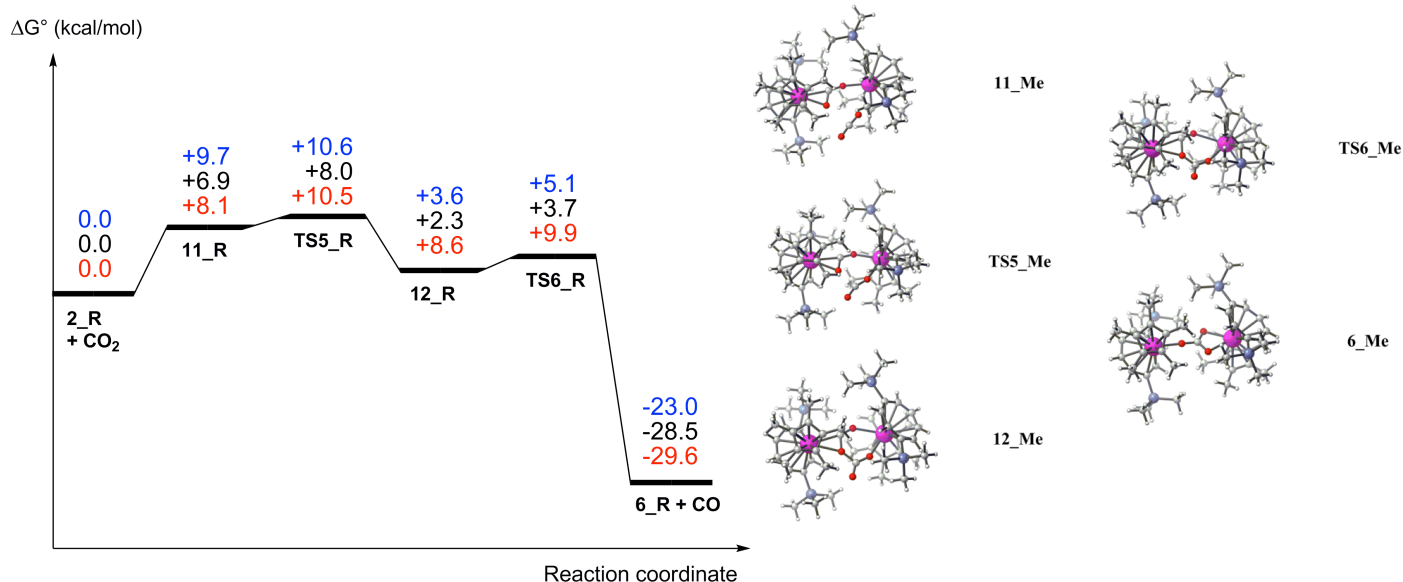
Figure 11. Computed free energy profile of reaction mechanism **M2** between **1_R** (R = H in red, R = Me in blue, R ^{t}Bu in black) and CO_2 (left). Computed structures for R = Me (left). Structures with R = H are qualitatively similar. (uranium : pink, carbon : grey, hydrogen = white, oxygen = red, silicon = blue)

carbonate complex **6_Me**. Again, there is no important steric repulsion and the activation barrier is low (+5.1 Kcal/mol, with respect to **2_Me**) and the formation of the carbonate complex is exergonic by -23.0 Kcal/mol, as seen above. This pathway is thus energetically very smooth and leads easily to the formation of the bimetallic carbonate complex. Since intermediate **12_Me** is unstable and **TS6_Me** is lower in energy than **TS5_Me**, the entire pathway can be seen as a concerted mechanism. The electrophilic attack of CO_2 is concomitant with the release of CO. Mechanism **M2** presents also a lower activation barrier (+8.0 Kcal/mol) for the formation of the carbonate dimer when R = ^{t}Bu, demonstrating that mechanism **M1** is not competitive. This is in excellent agreement with the experiments since the μ-oxo complex is never observed with R = ^{t}Bu.

The formation of the oxalate complex has also been computed through mechanism **M3**. The computed free energy profile of this reaction and the corresponding geometries are presented in Figure 12. The transition state for the C-C coupling between the free CO_2 molecule and the CO_2^{2-} moiety of **2_Me** presents an activation barrier of +16.6 Kcal/mol with respect to **2_Me** making this reaction kinetically slightly less favorable than the formation of the carbonate *via* mechanism **M2**. Since the U-U distance is still long at **TS7_Me**, this difference of barrier is not due to steric effects but electronic ones. Indeed, it is more difficult to make a bond between two positively charged carbon atoms than between a positively charged carbon and a negatively charged oxygen as in **TS5_Me** (Figure 11). On the other hand, the formation of the oxalate dimer **14_Me** is exergonic by -54.3 Kcal/mol, which is thermodynamically more favorable than the corresponding carbonate and CO (-28.5 Kcal/mol, Figure 11). Calculated structural parameters are in
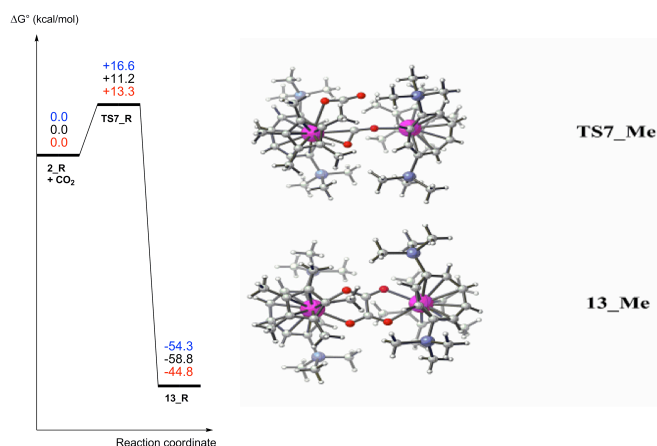

Figure 12: Computed free energy profile of reaction mechanism **M3** between **1_R** (R = H in red, R = Me in blue, R = ^{t}Bu in black) and CO_2 (left). Computed structures linked to the energy profile for R=Me (right). Structures with R = ^{t}Bu are qualitatively similar. (uranium : pink, carbon : grey, hydrogen = white, oxygen = red, silicon = blue)

good agreement with the experiments in both cases, and a pictorial comparison is provided in the ESI. Globally, bond lengths involving uranium are longer in our calculations because of the use of the large core pseudopotential and the lack of core-valence polarization.[45] The important energetic data of the four computed pathways are summarized in Table 6.

Experimentally, the reaction between [U(η^8-C_8H_6{SiMe$_3$-1,4}$_2$)(η^5-C_5Me_5)] (**1_Me**) and CO_2 leads to the formation of

the μ-oxo dimer (**6**) (*via* mechanism **M1** starting from **7_Me** (Figure 8)) and the oxalate dimer (**7**) (*via* mechanism **M3** (Scheme 3)). Barriers of +15.4 Kcal/mol and +16.6 Kcal/mol for mechanism **M1** starting with **7_Me** and **M3** respectively are overcome since the oxo and the oxalate products are observed experimentally. The thermodynamic driving force is definitively more important for mechanism **M3** (-54.3 kcal/mol) but the formation of the oxalate complex is a bimolecular process while the formation of the oxo complex is a monomolecular process. Thus the formation of the oxalate relies upon the meeting of **2_Me** with CO_2 while the formation of the oxo does not. This is the reason why both products are observed experimentally, although both mechanisms present two equivalent activation barriers but very different free

distance remains long, releasing steric repulsion. It is not clear why the oxalate product is not observed with R = ^tBu since the activation barrier of mechanism **M3** is accessible, and only 3.2 kcal/mol higher than the one of mechanism **M2**. In this respect, it is important to note that the systematic error of the DFT method is ca. 2 Kcal/mol (when introducing dispersion corrections, as is the case in this study), whereas experimentally a difference of more than 1 Kcal/mol between two activation barriers can be enough to favor one mechanism over another.[46]

	First TS	Intermediate	Second TS	Products
R = Me				
Mechanism M1 starting with **2_Me**	+35.9	+11.8	+25.3	-23.0
Mechanism M1 starting with **7_Me**	+15.4	-12.5	+1.2	-30.4
Mechanism M2	+10.6	+3.6	+5.1	-23.0
Mechanism M3	+16.6	-	-	-54.3
R = ^tBu				
Mechanism M1 starting with **2_tBu**	+35.3	+15.4	+26.3	-28.5
Mechanism M1 starting with **7_tBu**	+26.0	-2.1	+21.2	-23.5
Mechanism M2	+8.0	+2.3	+3.7	-28.5
Mechanism M3	+11.2	-	-	-58.8

Table 6. Summary of Computed Energetic Data

energies of reaction. Although the carbonate dimer is predicted either *via* mechanism **M1** or **M2** such a compound has not so far been isolated experimentally. At this point it should be pointed out that the oxalate dimers discussed above precipitate out of the reaction solution, thus providing an extra driving force to the reaction and altering the kinetics of the overall transformation (e.g. faster depletion of CO_2 in the oxalate route). Nevertheless the observation of the carbonate dimes in the case of the reactions of [U(η^8-C_8H_6{SiMe$_3$-1,4}$_2$)(η^5-Cp^{Me4Et})(THF)] (**2**) and [U(η^8-C_8H_6{SiMe$_3$-1,4}$_2$)(η^5-Cp^{Me4iPr})(THF)] (**3**) with CO_2 supports the validity of mechanism **M2** or **M1** (the latter starting from the corresponding **7_R** intermediates). Similarly in the case of **1_tBu**, the formation of the μ-oxo complex is also less thermodynamically favorable (-2.1 kcal/mol) and mechanisms **M2** or **M3** both present lower activation barriers (+8.0 Kcal/mol and +11.2 Kcal/mol, respectively), making mechanism **M1** not competitive. As mentioned above the μ-oxo dimer is not observed but unfortunately neither is the oxalate despite being the most stable product according to the calculations (free energy of reaction = -58.8 kcal/mol). That would mean that only mechanism **M2** operates experimentally for R = ^tBu. It is indeed a very easy pathway as the U-U

Conclusions

In summary, we have shown that manipulation of the steric environment around the uranium center plays a crucial role in determining the possible reductive reaction pathways between complexes of the type [U(η^8-C_8H_6{SiMe$_3$-1,4}$_2$)(η^5-Cp^{Me4R})(THF)$_x$] (x = 0,1; R = Me, Et, ^iPr, ^tBu) and CO_2. This has led to the first example of reductive coupling of CO_2 to oxalate using an organo-actinide complex. The synthetic work has been corroborated by cyclic voltammetery studies, which show that the reductive strength of the aforementioned complexes is essentially the same within the series, and by a detailed mechanistic DFT study. The latter exemplifies the synergy between experiment and theory that is crucial in order to understand and rationalize the observed reactivity.

Acknowledgements

Notes and references

[a] Department of Chemsitry, School of Life Sciences, University of Sussex, Brighton BN1 9QJ, UK; f.g.cloke@sussex.ac.uk

[b] LPCNO, Université de Toulouse, INSA Toulouse,135 Avenue de Rangueil, 31077 Toulouse; laurent.maron@irsamc.ups-tlse.fr

1 *Activation of Small Molecules: Organometallic and Bioinorganic Perspectives,* Wiley-VCH, 2006; *Homogeneous Catalysis: Understanding the Art*, Kluwer Academic, 2003

2 *Carbon Dioxide as a Chemical Feedstock,* Wiley, 2010

3 E. Balaraman, C. Gunanathan, J. Zhang, L. J. Z. Shimon, D. Milstein, *Nat. Chem.,* 2011, **3,** 609-614.

4 C. Finn, S. Schittger, L. J. Yellowlees, F. White, J. B. Love, *Chem. Commun.,* 2012, **48,** 1392.

5 D. W. Stephan, *Dalton Trans.,* 2009, 3129.; A. A. Ashley, A. L. Thomson, D. O Hare, *Angew. Chem. Intl. Ed.,* 2009, **48,** 9839.; A. A. Ashley, D. O Hare, *Topics in Current Chemistry,* 2013, **334,** 191-217.

6 S. N. Riduan, Y. Zhang, *Dalton Trans.,* 2010, **39,** 3347.; Y. Tsuji, T. Fujihara, *Chem. Commun.,* 2012, **48,** 9956.; T. Sakakura, J.-C. Choi, H. Yasuda, *Chem. Rev.,* 2007, **107,** 2365-2387.; K. Huang, C.-L. Sun, Z.-J. Shi, *Chem. Soc. Rev,* 2011, **40,** 2435.

7 P. L. Arnold, *Chem. Commun.,* 2011, **47,** 9005.; T. Andrea, M. S. Eisen, *Chem. Soc. Rev,* 2008, **37,** 550.; M. Ephritikhine, *Organometallics,* 2013, **32,** 2464; B. M. Gardner and S. T. Liddle, *Eur. J. Inorg. Chem.,* 2013, **22-23,** 3753-3770; H. S. La Pierre and K. Meyer, *Prog. Inorg. Chem.,* 2014, **58,** 303–416.

8 P. Russel, P. J. Scott, *J. Am. Chem. Soc.,* 1998, **120,** 1070.; F. G. N. Cloke, P. B. Hitchcock, *J. Am. Chem. Soc.,* 2002, **124,** 9352.; S. M. Mansell, N. Kaltsoyannis, P. L. Arnold, *J. Am. Chem. Soc.*, 2011**, 133,** 9036.

9 O. T. Summerscales, F. G. N. Cloke, P. B. Hitchcock, J. C. Green, N. Hazari, *Science,* 2006, **311,** 829.; O. T. Summerscales, F. G. N. Cloke, P. B. Hitchcock, J. C. Green, N. Hazari, *J. Am. Chem. Soc.,* 2006, **128,** 9502.; P. L. Arnold, Z. B. Turner, R. M. Bellabarda, R. P. Tooze, *Chem. Sci.,* 2011, **2,** 77.; B. M. Gardner, J. C. Stewart, A. L. Davis, J. McMaster, W. Lewis, A. J. Blake, S. T. Liddle, *Proc. Natl. Acad. Sci.,* 2012, **109,** 9265.; A. S. Frey, F. G. N. Cloke, P. B. Hitchcock, I. J. Day, J. C. Green, G. Aitken, *J. Am. Chem. Soc.,* 2008, **130,** 13816.; G. J. Brennan, R. A. Andersen, J. L. Robbins, *J. Am. Chem. Soc.,* 1986, **108,** 335.

10 N. Tsoureas, O. T. Summerscales, F. G. N. Cloke, S. M. Roe, *Organometallics,* 2013, **32,** 1353.

11 A. S. Frey, F. G. N. Cloke, M. P. Coles, L. Maron, T. Davin, *Angew. Chem. Intl. Ed.,* 2011, **50**, 6881.

12 I. Castro-Rodriguez, K. Meyer, *J. Am. Chem. Soc.*, 2005, **127,** 11242.

13 V. Mougel, C. Camp, J. Pécaut, C. Copéret, L. Maron, C. E. Kefalidis and M. Mazzanti, *Angew. Chem. Intl. Ed.,* 2012, **51,** 12280–12284; O. Cooper, C. Camp, J. Pécaut, C. E. Kefalidis, L. Maron, S. Gambarelli, M. Mazzanti, *J. Am. Chem. Soc.,*published on the web 08 April 2014, **DOI:** 10.1021/ja5017624.

14 O. T. Summerscales, A. S. Frey, F. G. N. Cloke, P. B. Hitchcock, *Chem. Commun.,* 2009, 198.

15 O. P. Lam, S. C. Bart, H. Kameo, F. W. Heinemann and K. Meyer, *Chem. Commun.,* 2010,**46,** 3137-3139; A.-C. Schmidt, A. V. Nizovtsev, A. Scheurer, F. W. Heinemann and K. Meyer, *Chem. Commun.,* 2012, **48,** 8634-8636.

16 F. A. Henglein, H. Sontheimer, *Z. fuer Anorg. und Allg. Chemie,* 1951 , **267,** 181 – 188.

17 C. T. Saouma, C. C. Lou, M. W. Day, J. C. Peters, *Chem. Sci.,* 2013, **4,** 4042; C. T. Saouma, C. C. Lou, M. W. Day, J. C. Peters, *J. Am. Chem. Soc.*, 2007, **129,** 4.

18 L. J. Farrugia, S. Lopinski, P. A. Lovatt, R. D. Peacock, *Inorg. Chem.,* 2001, **40,** 558.

19 W. J. Evans, C. A. Seibel, J. W. Ziller, *Inorg. Chem.,* 1998, **37,** 770.

20 W. J. Evans, J. M. Perotti, J. C. Brady, J. W. Ziller, *J. Am. Chem. Soc.*, 2003, **125,** 5204.

Chemical Science Accepted Manuscript

[21] W. J. Evans, S. E. Lorenz, J. W. Ziller, *Inorg. Chem.,* 2009, **48,** 2001.

[22] L. R. Avens, C. J. Burns, R. J. Butcher, D. L. Clark, J. C. Gordon, A. R. Schake, B. L. Scott, J. G. Watkin, B. D. Zwick, *Organometallics,* 2000, **19,** 451.

[23] A. S. P. Frey, F. G. N. Cloke, M. P. Coles, P. B. Hitchcock, *Chem. Eur. J.,* 2010, **16,** 9446.

[24] A. E. Bradley, C. Hardacre, M. Nieuwenhuyzen, W. R. Pitner, D. Sanders, K. R. Seddon, R. C. Thied, *Inorg. Chem.,* 2004, **43,** 2503.

[25] G. A. Jeffrey, G. S. Parry, *J. Am. Chem. Soc.*, 1954, **76,** 5283.

[26] J. Fujita, K. Nakamoto, M. Kobayashi, *J. Phys. Chem.*, 1957, **61,** 1014.

[27] In the case of (**9**), the identity of the compound was further established *via* its independent synthesis from $[U(\eta^8\text{-}C_8H_6\{SiMe_3\text{-}1,4\}_2)(\eta^5\text{-}Cp^{Me4iPr})Cl]$ (**10**) and 0.5 eq $Tl_2C_2O_4$ in toluene (see ESI for further details). Thus (**9**)-^{12}C prepared this way had an identical ^{1}H-NMR spectrum to that of (**9**) prepared from $^{13}CO_2$.

[28] C. L. Webster, J. W. Ziller, W. J. Evans, *Organometallics,* 2014, **33,** 433.

[29] T. E. Hanna, E. Lobkovsky, P. J. Chirik, *Organometallics,* 2009, **28,** 4079.

[30] J. Okuda, R. W. Albach, E. Herdtweck, F. E. Wagner, *Polyhedron,* 1991, **10,** 1741.

[31] B. C. Baker, D. T. Sawyer, *Inorg. Chem.,* 1970, **9,** 197

[32] D. W. Wester, J. C. Sullivan, *Inorg. Chem.,* 1980, **19,** 2838.

[33] C. Clappe, D. Leveugle, D. Hauchard, G. Durand, *J. Electr. Chem.,* 1998, **448,** 95.

[34] C. R. Graves, P. Yang, S. A. Kozimor, A. E. Vaughn, D. L. Clark, S. D. Conradson, E. J. Schelter, B. L. Scott, J. D. Thompson, P. J. Hay, D. E. Morris, J. L. Kiplinger, *J. Am. Chem. Soc.*, 2008, **130,** 5272.

[35] D. Hauchard, M. Cassir, J. Chivot, *J. Electr. Chem.,* 1991, **313,** 227.

[36] B. Kosog, H. S. La Pierre, F. W. Heinemann, S. T. Liddle, K. Meyer, *J. Am. Chem. Soc.*, 2012**, 134,** 5284.

[37] R. G. Compton and C. E. Banks, *Understanding Voltammetry,* Imperial College Press, 2nd Edn., 2011.

[38] A.-C. Schmidt, A. V. Nizovtsev, A. Scheurer, F. W. Heinemann, K. Meyer, *Chem. Commun.,* 2012**, 48,** 8634.

[39] L. Castro, O.P. Lam, S.C. Bart, K. Meyer, L. Maron, *Organometallics,* 2010, **29,** 5504.

[40] O. P. Lam, L. Castro, B. Kosog, F. W. Heinemann, L. Maron, K. Meyer, *Inorg. Chem.,* 2012, **51,** 781.

[41] L. Castro, S. Labouille, D. R. Kindra, J. W. Ziller, F. Nief, W. J. Evans, L. Maron, *Chem. Eur. J.*, 2012, **18,** 7886.

[42] L. Castro, L. Maron, *Chem. Eur. J.,* 2012, **18,** 6610.

[43] D. McKay*,* A. S. P. Frey, J. C. Green, F. G. N. Cloke, L. Maron*. Chem*. *Commun*., 2012, **48,** 4118.

[44] S. Labouille, F. Nief, L. Maron, *J. Phys. Chem. A,* 2011, **115,** 8295.

[45] L. Castro, A. Yahia, L. Maron*, Dalton Trans.,* 2010, **39,** 6682.; C. E. kefalidis, A. S. P.Frey, S. M. Roe, F. G. N. Cloke, L. Maron, *Dalton Trans.,* published on the web 04/04/2014, **DOI:** 10.1039/C4DT00618F.;

[46] M.-C. Kim, E. Sim, K. Burke, *Phys. Rev. Lett.,* 2013, **111,** 073003.; K. Burke, *J. Chem. Phys.,* 2012, **136,** 150901.; *Computational Methods for Large Systems,* Wiley, 2010.

Chemical Science Accepted Manuscript